Published in final edited form as:
J Control Release. 2011 February 10; 149(3): 323–331. doi:10.1016/j.jconrel.2010.10.031.

Enhanced Endothelial Delivery and Biochemical Effects of α-Galactosidase by ICAM-1-Targeted Nanocarriers for Fabry Disease

Janet Hsu[a,‡], **Daniel Serrano**[b,‡], **Tridib Bhowmick**[c], **Kishan Kumar**[d], **Yang Shen**[e], **Yuan Chia Kuo**[a], **Carmen Garnacho**[c], and **Silvia Muro**[a,c,*]

[a] Fischell Department of Bioengineering, School of Engineering, University of Maryland College Park, College Park, MD 20742, USA

[b] Cell Biology and Molecular Genetics, College of Chemical and Life Sciences, University of Maryland College Park, College Park, MD 20742, USA

[c] Center for Biosystems Research, University of Maryland Biotechnology Institute, College Park, MD 20742, USA

[d] Biotechnology Program, School of Engineering, University of Pennsylvania, Philadelphia, PA 19104, USA

[e] Molecular and Cell Biology, College of Chemical and Life Sciences, University of Maryland College Park, College Park, MD 20742, USA

Abstract

Fabry disease due to deficiency of α-galactosidase A (α-Gal) causes lysosomal accumulation of globotriaosylceramide (Gb3) in multiple tissues and prominently in the vascular endothelium. Although enzyme replacement therapy (ERT) by injection of recombinant α-Gal improves the disease outcome, effects on the vasculopathy associated to life-threatening cerebrovascular, cardiac and renal complications are still limited. We designed a strategy to enhance delivery of α-Gal to organs and endothelial cells (ECs). We targeted α-Gal to intercellular adhesion molecule 1 (ICAM-1), a protein expressed on ECs throughout the vasculature, by loading this enzyme on nanocarriers coated with anti-ICAM (anti-ICAM/α-Gal NCs). *In vitro* radioisotope tracing showed efficient loading of α-Gal on anti-ICAM NCs, stability of this formulation under storage and in model physiological fluids, and enzyme release in response to lysosome environmental conditions. In mice, delivery of ^{125}I-α-Gal was markedly enhanced by anti-ICAM/^{125}I-α-Gal NCs in brain, kidney, heart, liver, lung, and spleen, and transmission electron microscopy showed anti-ICAM/α-Gal NCs attached to and internalized into the vascular endothelium. Fluorescence microscopy proved targeting, endocytosis and lysosomal transport of anti-ICAM/α-Gal NCs in macro- and micro-vascular ECs, and a marked enhancement of Gb3 degradation. Therefore, ICAM-1-targeting strategy may help improve the efficacy of therapeutic enzymes for Fabry disease.

[*]Correspondence should be addressed to: Silvia Muro, Center for Biosystems Research, 5115 Plant Sciences Building, College Park, MD 20742-4450., Tel. 1+301-405-4777., Fax. 1+301-314-9075., muro@umd.edu.
[‡]The first two authors contributed equally to this work.

Keywords

Vascular endothelium; Fabry disease; ICAM-1 targeting; polymer nanocarriers; α-Gal enzyme replacement therapy

INTRODUCTION

Fabry disease is a lysosomal storage disorder (LSD) caused by a genetic deficiency of α-galactosidase A (α-Gal) [1]. This enzyme hydrolyzes terminal α-D-galactosyl residues from neutral glycosphingolipids transported into lysosomes from the blood, plasma membrane and intracellular compartments [1]. As a result of the enzyme deficiency, blood group B substances, galabiosylceramide, and mainly globotriaosylceramide (Gb3) accumulate in body fluids and tissue lysosomes [1]. Gb3 deposits are found in endothelial, perithelial, and smooth-muscle cells in the vasculature, cells of the reticuloendothelial and myocardial tissues, renal epithelial cells, and perineural cells of the autonomic nervous system, causing multi-organ dysfunction and premature death [1].

The clinical manifestations of Fabry disease are variable, yet life-threatening complications commonly arise from progressive cerebrovascular, cardiac and renal impairments caused by the prominent vasculopathy [1]. Vascular lesions lead to myocardial ischemia, hypertension, atherogenesis, stroke, aneurysm, thrombosis, and renal failure [1]. The lung function can also be compromised by airflow obstruction, edema, and pulmonary embolism [1]. These effects of the vasculopathy typical of Fabry disease are strongly associated with endothelial dysfunction, and hence, endothelial cells (ECs) are a main target for therapeutic intervention of this malady [1–3].

An available treatment for Fabry disease is enzyme replacement therapy (ERT) using recombinant galactosidases that contain mannose-6-phosphate (M6P) [4]. They can bind to M6P receptors on the surface of cells and be transported to lysosomes via clathrin-coated pits [5,6]. When injected in the circulation, these enzymes accumulate in tissues and attenuate Gb3 levels [7–10]. However, despite clear utility of ERT, patients show varying effects and modest response to vasculopathy in the cardiovascular and neurological systems [11,12]. Altered expression or function of M6P receptors in cells affected by LSDs and formation of immune-complexes that impair enzyme binding to cell receptors may contribute to limit ERT outcome [13–16].

Efficacy of ERT for Fabry disease may benefit from strategies enhancing enzyme delivery to organs and vascular ECs via M6P-independent pathways. Targeting of α-Gal to intercellular adhesion molecule 1 (ICAM-1) may help accomplish this goal. ICAM-1 is a transmembrane glycoprotein and an adhesion molecule for leukocytes in inflammation [17]. It is expressed on vascular ECs and other cells in the body, and its expression is upregulated under pathology, including Fabry disease [18,19]. ICAM-1 can be targeted by antibodies and affinity peptides for delivery of protein conjugates, contrast and therapeutic agents, and drug delivery vehicles such as liposomes and polymer nanocarriers in cells and animals [20–31].

We have shown that ICAM-1-targeted nanocarriers efficiently enhanced delivery of acid sphingomyelinase (ASM, a lysosomal enzyme deficient in types A-B Niemann-Pick disease) to mouse organs and macrovascular ECs [23,26,27]. ASM trafficked to lysosomes by cell adhesion molecule- (CAM)-mediated endocytosis, bypassing clathrin-mediated uptake utilized by current ERTs [27]. Yet, the efficacy of this strategy to enhance the delivery of α-Gal or other enzymes and the degree of such enhancement are unpredictable. Different

efficacy patterns can arise from potential variations in the enzyme loading capacity of nanocarriers and/or different enzyme pharmacokinetics, which are in part imposed by biochemical properties of the enzyme itself. In addition, delivery of lysosomal enzymes to microvascular ECs (the major endothelial surface in the body, phenotypically and functionally different from macrovascular ECs) [32,33], has not been tested. Whether ECs with Gb3 storage typical of Fabry disease can efficiently internalize and transport nanocarriers to lysosomes also remains to be determined.

In this work, we have loaded α-Gal on model ICAM-1-targeted nanocarriers (anti-ICAM/α-Gal NCs) and used radioisotope tracing, fluorescence and electron microscopy to study this formulation *in vitro*, cell cultures and animals in comparison to non-targeted α-Gal. Our results demonstrate: (a) stability of anti-ICAM/α-Gal NCs under storage and enzyme release in response to lysosome environmental conditions, (b) enhanced enzyme delivery to organs and targeting to ECs in mice, and (c) efficient endocytosis, lysosomal transport, and Gb3 degradation in a Fabry disease model of micro- and macro-vascular ECs.

MATERIALS AND METHODS

Antibodies and reagents

Monoclonal antibodies to human or mouse ICAM-1 (anti-ICAM) were R6.5 and YN1, respectively [26]. Secondary antibodies were from Jackson Immunoresearch (West Grove, PA). Neutral α-Gal from *E. coli* (Calbiochem; San Diego, CA) or coffee bean (Sigma Aldrich; St. Louis, MO) were chosen to distinguish this activity from the endogenous acidic lysosomal counterpart. α-Gal from *E. Coli* was used in experiments in cell culture. α-Gal from coffee bean was used in experiments requiring ^{125}I labeling and in functional activity assays. fluorescein isothiocyanate (FITC)-labeled and non-fluorescent 100 nm diameter polystyrene particles were from Polysciences (Warrington, PA). Cell media and supplements were from Cellgro (Manassas, VA) or Gibco BRL (Grand Island, NY). Na^{125}I and Pierce Iodination Beads were from Perkin Elmer - Analytical Sciences (Wellesley, MA) and Thermo Scientific (Rockford, IL). All other reagents were from Sigma Aldrich (St. Louis, MO).

Preparation of anti-ICAM/α-Gal nanocarriers and enzyme release

Prototype anti-ICAM/α-Gal NCs were prepared by adsorbing anti-ICAM or a mix of anti-ICAM and α-Gal (95:5 or 50:50 antibody-to-enzyme mass ratio) onto the surface of 100-nm diameter polystyrene particles, as described [27]. Where indicated, a mix of anti-ICAM and ^{125}I-α-Gal was used to trace the enzyme cargo (95:5 unlabeled-to-labeled enzyme molar ratio) [23]. Non-bound counterparts were separated by centrifugation [23]. The final diameter of the particles was kindly measured by NanoSight Limited using Nanoparticle Tracking Analysis (NanoSight LM20 System, Salisbury, Wilshire, UK).

Release of ^{125}I-α-Gal from anti-ICAM/^{125}I-α-Gal NCs was determined at 30 min, 1, 5, 8, 24, 48, and 72 h after particle preparation by centrifugation to separate free enzyme from particle-bound fraction. Release was assessed after 2 rounds of centrifugation at 13.8 g, resuspension by pipetting, and sonication. Enzyme release was also tested during incubation in storage buffer (phosphate buffer saline, PBS, supplemented with 1% bovine serum albumin, BSA), complete cell medium (described below), or fetal bovine serum (FBS), at 4°C or 37°C, pH 7.4 or pH 4.5, and in absence or presence of enzyme substrate analog (2 μg/ml N-Dodecanoyl-NBD-ceramide trihexoside, NBD-Gb3; Matreya, LLC, Pleasant Gap, PA).

Pharmacokinetics and visualization of anti-ICAM/α-Gal nanocarriers in mice

Anesthetized C57BL/6 mice (Jackson Laboratory, Bar Harbor, Maine) were injected intravenously with ^{125}I-α-Gal or anti-ICAM/^{125}I-α-Gal NCs to track biodistribution of the enzyme, and FITC-labeled anti-ICAM/α-Gal NCs to track carrier particles (30 μg/kg α-Gal, 1.5X10^{13} particles/kg). Blood was collected from the retro-orbital sinus 1, 15, and 30 min after injection. Brain, heart, kidneys, liver, lungs, and spleen were collected 30 min or 24 h after injection. Alternatively, a set of animals was perfused with PBS prior to organ collection to eliminate blood and the circulating nanocarrier fraction. The radioactivity and weight of the samples were determined to calculate the following parameters: percentage of injected dose (%ID), percentage of injected dose per gram of tissue to compare among organs of different size (%ID/g), localization ratio to compare tissue-to-blood distribution (LR; %ID/g organ: %ID/g in blood), and specificity index to compare targeted-to-non-targeted counterparts (SI; LR of anti-ICAM/α-Gal NCs: LR of α-Gal). For fluorescence measurements organ sections were imaged by confocal microscopy (Leica TCS SP5 X) using Leica Lite 2.0.2 Software (Leica Microsystems, Wetzlar, Germany). For transmission electron microscopy (TEM) studies, organs were fixed in 2.5% glutaraldehyde and 0.1 M sodium cacodilate buffer and processed from 80–90 nm thin resin-embedded sections [26]. These studies were performed according to IACUC and University regulations.

In vivo ICAM-1 expression

To complete previous data on ICAM-1 expression in mice [23], brain was collected from C57Bl/6 mice and homogenized at 4°C in lysis solution (1x pheylmethylsulfonyl fluoride, 1x protease inhibitor cocktail, 0.5% sodium dodecyl sulfate, and 0.5% Triton X-100 in PBS). Protein electrophoresis, membrane transfer, immunoblot with rat anti-mouse ICAM, chemiluminiscence detection with horseradish peroxidase-conjugated goat anti-rat immunoglobulin G (IgG), and protein band densitometry were performed as described [23]. Data were normalized to actin levels, used as a control [23].

Cell culture models

Human umbilical vein endothelial cells (HUVECs; Clonetics, San Diego, CA) were cultured in M-199 media supplemented as described [34]. Human brain microvascular endothelial cells (HBMECs; Applied Cell Biology Research Institute, Kirkland, WA) were cultured at 37ºC, 5% CO_2 and 95% humidity in RPMI-1640 supplemented with 20% fetal bovine serum (FBS), 2 mM glutamine, 30 μg/mL endothelial cell growth supplement, 100 μg/mL heparin, 100 U/mL penicillin and 100 μg/mL streptomycin. Cells were seeded on 1% gelatin-coated glass coverslips, and activated for 16 h with 10 ng/mL TNFα (tumor necrosis factor α; BD Biosciences, Franklin Lakes, NJ).

Where indicated, cells were additionally incubated for 16 h in 50, 200, 400, 500 or 1000 μM deoxygalactonojirimycin hydrochloride (DGJ) to inhibit endogenous α-Gal and mimic lysosomal Gb3 storage of Fabry disease. Given that 500 μM DGJ was sufficient to achieve this goal, this concentration was used in subsequent experiments. Gb3 accumulation was verified by incubating cells with a fluorescent analog (2–10 μg/mL NBD-Gb3), followed by fixation in cold 2% paraformaldehyde, and imaging in a fluorescence microscope (Olympus IX81, Olympus, Inc., Center Valley, PA), using a 40X objective (UPlanApo, Olympus, Inc.) and 4′,6-diamidino-2-phenylindole (DAPI), FITC, and Texas-Red filters (1160A-OMF, 3540B-OMF, 4040B-OMF; Semrock, Inc., Rochester, NY). Micrographs were taken with an ORCA-ER camera (Hamamatsu Corporation, Bridgewater, NJ) and SlideBook 4.2 software (Intelligent Imaging Innovations, Inc., Denver, CO). Fluorescence images were analyzed using Image-Pro 6.3 software (Media Cybernetics, Inc., Bethesda, MD).

Targeting and internalization of anti-ICAM/α-Gal nanocarriers

TNFα activated HUVECs or HBMECs (treated or not with 500μM DGJ to mimic Fabry disease) were incubated at 37°C for 30 min with FITC-labeled anti-ICAM NCs or anti-ICAM/α-Gal NCs (2.5 μg/mL α-Gal, 7×10^{10} particles/mL), followed by washing off non-bound nanocarriers and incubation in cell medium for an additional 30-min period. Similar experiments were conducted in medium containing 3 mM amiloride (an inhibitor of CAM-mediated endocytosis) or 50 μM monodansylcadaverine (MDC, an inhibitor of clathrin-mediated endocytosis). After cell fixation, surface-bound nanocarriers were stained with Texas-Red-labeled goat anti-mouse IgG and nuclei were stained with DAPI. Samples were imaged by fluorescence microscopy to determine the total number of FITC-labeled nanocarriers associated per cell, and the percentage of nanocarriers which localized at the cell surface or were internalized (Texas-Red-positive vs Texas-Red-negative nanocarriers), as previously described [34]. Phase-contrast was used to delimit the cell borders.

Intracellular destination of anti-ICAM/α-Gal nanocarriers

HUVEC lysosomes were labeled with Texas-Red dextran (10,000 MW), as described [25]. Cells were then incubated with FITC-labeled anti-ICAM/α-Gal NCs for 1 h at 37°C, followed by washing off non-bound nanocarriers. Cells were fixed at that point or subjected to additional incubation in cell medium up to a final time of 3 or 5 h. Samples were analyzed by fluorescence microscopy to determine the percentage of FITC-labeled nanocarriers that colocalized with Texas-Red-positive lysosomes [25].

DGJ-treated HUVECs were incubated for 16 h at 37°C with 10 μg/mL NBD-Gb3 (green fluorescence), washed and incubated with non-fluorescent anti-ICAM/α-Gal NCs (2.5 μg/mL αGal, 7×10^{10} particles/mL) for 1 h. Non-bound carriers were removed and cells were fixed or incubated with medium for additional time, up to 3 or 5 h. Cells were fixed, permeabilized and incubated with Texas-Red-labeled goat anti-mouse IgG to stain carriers in red. Colocalization of nanocarriers with Gb3-positive compartments was assessed by fluorescence microscopy.

Functional activity of anti-ICAM/α-Gal nanocarriers

TNFα activated HUVECs were incubated with 500 μM DGJ and 2 μg/mL NBD-Gb3 (green fluorescence) to induce lysosomal Gb3 storage. Cells were then incubated with cell medium, α-Gal, or anti-ICAM/α-Gal NCs for 5 h in the presence of 300 μM chloroquine. Chloroquine is a mild base used to inhibit the activity of endogenous α-Gal, an acidic enzyme, while allowing activity of neutral α-Gal loaded on anti-ICAM NCs (2.5 μg/mL α-Gal, 7×10^{10} particles/mL). Degradation of NBD-Gb3 in the disease cell model was assessed by fluorescence microscopy and compared to control cells as follows:

$$\%\ \text{Gb3 degradation} = 100 \times \left\{ 1 - \frac{(\text{Gb3 in diseased cells after treatment} - \text{Gb3 in control cells})}{(\text{Gb3 in diseased cells} - \text{Gb3 in control cells})} \right\}$$

Statistics

Data were calculated as mean ± standard error of the mean (SEM). Statistical significance was determined by Student's unpaired *t*-tests.

RESULTS

Characterization of anti-ICAM/α-Gal nanocarriers and enzyme release

As a proof-of-principle for nanocarrier-assisted targeting of enzymes for treatment of Fabry disease, both anti-ICAM targeting moiety and α-Gal enzymatic counterpart were coated on 100 nm nanocarriers (anti-ICAM/α-Gal NCs). The loading efficiency of ^{125}I-α-Gal was determined to be 76.6±4.1%, which rendered nanocarriers with 52.4±2.8 α-Gal molecules per particle and final diameter of 155±1.5 nm. The enzyme coat was stable under various physical stresses, including centrifugation, resuspension by pipetting, and sonication (11.6±0.3% enzyme release). Similarly, ^{125}I-α-Gal was stably retained on anti-ICAM NCs for up to 3 days of storage at 4°C in buffer solution (2.4±4.8% enzyme release at day 3; Fig. 1a). In addition, storage at 37°C did not cause a significant release from nanocarriers by day 3, compared to time 0 (11.8±0.9%; Fig. 1a).

Incubation of anti-ICAM/^{125}I-α-Gal NCs at 37°C in complete cell medium or serum (which mimic physiological fluids) showed a marked retention of ^{125}I-α-Gal on nanocarriers, with only 6.7±3.4% and 5.6±0.5% ^{125}I-α-Gal release at 1 h, and 8.0±3.8% and 11.3±1.9% release at 5 h (Fig. 1b). Enzyme release was significant after 3 day incubation in cell medium (14.8±2.0%) and a comparable release was seen after 8 h incubation in serum (19.5±1.6%). This suggests that although stable, α-Gal can be released from nanocarriers after delivery in cell culture or animal models. Supporting this, release at 37°C of ^{125}I-α-Gal from anti-ICAM NCs in cell medium was accelerated at pH 4.5, which mimics lysosomal pH (Fig. 1c). At acidic pH enzyme release was significant after only 5 h incubation (2.5±0.5%) vs 3 day incubation at neutral pH (Fig. 1c). Presence of substrate Gb3, typical of the final lysosomal destination of anti-ICAM/α-Gal NCs, further enhanced ^{125}I-α-Gal release (Fig. 1d). Under this condition, release at 5 h tripled that in the absence of substrate (7.2±0.7%), and reached a plateau (27.8±1.6%) by day 1 (Fig. 1d).

Pharmacokinetics and visualization of anti-ICAM/α-Gal nanocarriers in mice

We examined the potential of anti-ICAM/α-Gal NC strategy to deliver α-Gal to organs in the body that represent main targets for Fabry disease. The pharmacokinetics of anti-ICAM/^{125}I-α-Gal NCs was determined in anesthetized mice and compared to that of non-targeted ^{125}I-α-Gal. Anti-ICAM/^{125}I-α-Gal NCs disappeared from blood more rapidly than free ^{125}I-α-Gal: 5.9±0.7% of the injected dose (%ID) of nanocarriers was in blood 1–3 min after injection, while 42.1±2.2%ID of the free enzyme remained in circulation 30 min after injection (Table 1). Given that ^{125}I-α-Gal is traced in the nanocarrier samples, this result suggests the lack of significant release of the enzyme from nanocarriers in the circulation, confirming *in vitro* results obtained by incubation of nanocarriers in serum (Fig. 1B).

Fast accumulation in vascularized organs may account for rapid blood clearance of anti-ICAM/^{125}I-α-Gal NCs vs ^{125}I-α-Gal. Consistent with this, anti-ICAM/^{125}I-α-Gal NCs accumulated in all tested organs, as determined 30 min after injection, including brain, heart, kidney, liver, lung and spleen (Table 2). The liver and lungs (two of the largest and most heavily vascularized organs in the body, also presenting highest ICAM-1 expression [23]) received the largest fraction of anti-ICAM/^{125}I-αGal NC dose: 18.4±1.2%ID and 36.2±4.5%ID, vs 6.7±0.6%ID and 0.7±0.01%ID found in these organs in the case of non-targeted ^{125}I-α-Gal.

Normalization of the data per gram of tissue to compare uptake in organs of different size showed enhanced accumulation of anti-ICAM/^{125}I-α-Gal NCs in the lungs, 175.3±21.4%ID/g vs 12.4±0.7%ID/g in liver (Table 2). Since lungs contain a significant fraction of the total endothelium in the body (~10–30% [35–37]), preferential accumulation in this organ reflects endothelial specificity. In contrast, non-targeted ^{125}I-α-Gal accumulated similarly in these

two organs: 3.8±0.3%ID/g lung and 4.5±0.4%ID/g liver. Endothelial targeting of anti-ICAM/^{125}I-α-Gal NCs was also validated by comparison to control IgG NCs, reported to be ~10%ID/g lung vs ~50%ID/g liver [23,38].

Highlighting a high organ accumulation capacity, the organ-to-blood localization ratio (%ID/g in a tissue/%ID/g in blood) of anti-ICAM/^{125}I-α-Gal NCs was significantly higher than that of ^{125}I-α-Gal in all organs (ranging from 0.11±0.02 vs 0.03±0.002 in brain, to 70.1±12.0 vs 0.2±0.02 in the lungs) (Table 2). In addition, perfusion of mice prior to organ collection to eliminate circulating nanocarriers and those poorly bound to the vascular endothelium did not significantly decrease the amount of anti-ICAM/^{125}I-α-Gal NCs accumulated in organs, verifying effective organ targeting (Figure S1a).

Anti-ICAM/^{125}I-α-Gal NCs showed enhanced uptake in all organs vs non-targeted ^{125}I-α-Gal (Table 2). The highest fold increase or specificity index (localization ratio of the targeted vs non-targeted formulation) achieved was related to delivery of this enzyme to the liver, spleen, and lungs: 21.7-, 51.6-, and 367.8-fold increase, respectively. This accumulation of anti-ICAM/^{125}I-α-Gal NCs in the lungs decayed ~60% after 24 h, with a concomitant increase in the hepatic and splenic accumulation by that time (Figure S1). Despite such decay, the level of ^{125}I-α-Gal delivered to the lungs by anti-ICAM NCs was ~150 fold above that of non-targeted enzyme.

Although less prominent, a marked enhanced delivery to other major targets in Fabry disease was also achieved, e.g., kidney, brain, and heart delivery were enhanced by ~40%, 270%, and 410%. TEM of the heart and kidney tissues revealed anti-ICAM/α-Gal NCs bound to and internalized within cells of the endothelium in these organs, by 30 min after injection (Fig. 2).

Targeting and internalization of anti-ICAM nanocarriers in control micro- and macro-vascular endothelial cells and Fabry disease cell models

Vascular ECs are main targets for intervention in Fabry disease. Hence, a prerequisite for an efficient ERT delivery system for treatment of this malady is that it must efficiently target and enter both micro- and macro-vascular ECs. Data obtained in mice indicate that anti-ICAM/α-Gal NCs target the endothelium in the vasculature of all tested organs, yet the efficiency of anti-ICAM/α-Gal NCs to bind to and be internalized by micro- vs macro-vascular ECs is unknown. To assess this, binding and intracellular uptake of anti-ICAM NCs were tested for the first time in human microvascular ECs in comparison to human macrovascular ECs where these nanocarriers have been reported to be significantly efficient (~140 nanocarriers/cell, ~90% internalization) [34,38]. Anti-ICAM NCs behaved comparably in microvascular ECs in terms of binding (96.5±5.1% of macrovascular ECs) and internalization (86.8±2.7% of macrovascular ECs) (Fig. S2). Loading of α-Gal on anti-ICAM NCs did not affect the uptake efficiency of this delivery system by micro- or macro-vascular ECs: 109.4±5.5% and 91.0±1.6% of internalization of anti-ICAM NCs (Fig. 3a).

The internalization of anti-ICAM/α-Gal NCs was significantly inhibited by amiloride (54.8±2.8% of control), a pharmacological agent shown to disrupt CAM-mediated endocytosis, but not MDC (95.4±3.2% of control) [34], an inhibitor of clathrin-mediated endocytosis typically associated to the uptake of lysosomal enzymes (Fig. 3b). Therefore, the presence of α-Gal on anti-ICAM NCs did not affect the mechanism of internalization of this delivery system. Given that anti-ICAM NCs and anti-ICAM/α-Gal NCs showed similar targeting and internalization efficacy in both micro- and macro-vascular ECs, we limited the subsequent studies to one cell type: macrovascular ECs, for which we have historical control results.

Since Fabry disease notably affects the vascular endothelium, anti-ICAM/α-Gal NCs were tested in ECs mimicking this condition. To achieve pathological Gb3 accumulation, ECs were treated with increasing concentrations of DGJ, which inhibits α-Gal [39]. DGJ-treated cells displayed significant and dose-dependent intracellular storage of the fluorescent substrate analog NBD-Gb3 (Fig. S3).

Anti-ICAM/α-Gal NCs were also successful in targeting and internalizing in this Fabry-EC model: although their binding to cells was somewhat reduced (79.3±19.1% of control), this difference was not statistically significant and internalization of anti-ICAM/α-Gal NCs in the Fabry-EC model was slightly increased compared to control ECs (114.3±4.6%).

Lysosomal transport of anti-ICAM/α-Gal nanocarriers and attenuation of Gb3 storage in a Fabry disease cell model

The intended final destination of enzyme therapies for Fabry disease is the lysosome, where degradation of the Gb3 accumulated due to deficiency of α-Gal must take place. Intracellular trafficking of anti-ICAM/αGal NCs was examined by fluorescence microscopy to trace colocalization of internalized nanocarriers with fluorescent-dextran-loaded lysosomes (Fig. 4a). Dextran is a polysaccharide which cannot be enzymatically degraded in mammalian cells and, hence, stably accumulates in lysosomes, permitting their visualization [25].

As previously observed in the case of anti-ICAM NCs bearing other enzymatic cargoes [25,27], a majority of anti-ICAM/α-Gal NCs trafficked to endothelial lysosomes in a relatively short period of time: 27.4±3.4%, 73.5±2.1%, and 73.3±2.3% localization within lysosomes at 1, 3, and 5 h, respectively (Fig. 4a). In addition, anti-ICAM/α-Gal NCs were verified to colocalize with fluorescent NBD-Gb3 accumulated as a consequence of the DGJ-induced deficiency of lysosomal α-Gal: 29.3±3.4%, 31.0±3.8%, and 46.4±5.0% localization with Gb3 by 1, 3, and 5 h, respectively (Fig. 4b).

The efficacy of anti-ICAM/α-Gal NCs to reduce intracellular storage of Gb3 was tested in the EC model of Fabry disease and compared to that of untargeted α-Gal. In this model, after induction of intracellular Gb3 accumulation, DGJ must be removed to avoid inhibition of exogenous α-Gal.

We designed a method to ensure that Gb3 degradation is due to delivered α-Gal and not the endogenous α-Gal present in these cells. Exogenous α-Gal in our assays is a neutral enzyme, while endogenous lysosomal α-Gal in cells has acidic pK_a [1]. Treatment of disease-like ECs with αGal or anti-ICAM/α-Gal NC was assessed in the presence of chloroquine, which prevents lysosomal acidification and allows activity of the delivered, not the endogenous, enzyme.

As compared to normal ECs and diseased ECs incubated in the presence of sham medium (chloroquine was added as a control; Fig. 5a), treatment with untargeted α-Gal led to a slight, yet measurable, reduction of NBD-Gb3 by 5 h (32.4±1.5% reduction; Figs. 5a,b). This validates the method used and provides evidence of intracellular enzymatic activity in this Fabry-EC model. More importantly, degradation of Gb3 was significantly enhanced in cells treated with anti-ICAM/α-Gal NCs bearing a similar dose of α-Gal (68.9±5.0% reduction; Figs. 5a,b), suggesting that anti-ICAM NCs may be a viable option for targeted delivery of active therapeutic enzymes for Fabry disease.

DISCUSSION

The development of experimental treatments for Fabry disease and other LSDs is an active research field. ERT by infusion of recombinant α-Gal is one of the most successful

strategies currently available for treatment of Fabry disease [7–9]. However, limited response to common vasculopathy contributes to cerebrovascular, cardiac and renal complications, highlighting the need to optimize this approach [11,12].

Seminal work to improve the efficiency of therapeutic enzymes for treatment of LSDs date back four decades [40]. Coupling of model enzymes to polyethylene glycol was used to prolong the circulation of such enzymes in an attempt to enhance their uptake by tissues [41–43]. Encapsulation within neutral and charged liposomes was also explored to modulate the enzyme distribution and activity [41,43]. Coupling of liposomes to aggregated immunoglobulins or apolipoproteins was inspected in order to enhance their uptake by cells of the immune system in cases in which these cells represent a main target for intervention of LSDs [44,45]. However, apart from these initial studies, few other approaches have used drug carriers to control lysosomal enzyme delivery, despite the potential utility of this technology.

Currently, new biomaterials and nanotechnologies have allowed development of delivery systems that can increase the bioavailability of therapeutic agents, control their release rate, and provide targeting to sites in the body affected by disease [46–49]. These technologies seem well suited for intracellular delivery of protein therapeutics and ERT [23,27,50–52]. In this work we present proof-of-principle for a modality of enzyme delivery for Fabry disease assisted by targeted nanocarriers. In comparison with the non-targeted enzyme, this strategy improves the accumulation of α-Gal in mouse organs and ECs of the macro- and micro-vasculature, provides glycosylation-independent endocytosis and transport to lysosomes, and ultimately enhances attenuation of intracellular Gb3 storage.

In this model, α-Gal has been adsorbed on the surface of 100 nm polystyrene particles targeted with anti-ICAM. This configuration provides good loading efficiency (~75%), stable retention of the enzyme on the nanocarrier particle under storage and exposure to physiological conditions, and enzyme release in the lysosomal environment under presence of its substrate (Fig. 1). Importantly, α-Gal delivered into cells via anti-ICAM NCs notably enhanced (duplicated) Gb3 degradation compared to non-targeted α-Gal, supporting the potential of this strategy.

Although polystyrene nanoparticles used in this work are a prototype not intended for clinical use, they are a valid model to demonstrate α-Gal delivery by ICAM-1-targeted nanocarriers. In cell culture and laboratory animals, polystyrene particles display similar targeting and intracellular transport mechanisms than biocompatible poly(lactic-co-glycolic acid) nanocarriers, a material approved by the Food and Drug Administration [53]. They also present equivalent surface charge (~20 mV), allowing for similar efficacy and mechanism of enzyme adsorption [23,38].

Since lysosomal enzymes are only fully active in the acidic lysosomal environment, the enzymes loaded on the nanocarrier surface are “pro-drugs” until they reach this compartment and their encapsulation is not absolutely necessary. Enzyme exposure on the carrier surface may render fast recovery of activity upon delivery to lysosomes, as observed in our work (Figs. 4–5). The presence of α-Gal on the surface of anti-ICAM NCs did not notably affect the targeting and transport ability of these particles compared to nanocarriers whose entire surface is occupied by anti-ICAM. This was observed in cell culture where anti-ICAM/α-Gal NCs bind to and are endocytosed by ECs with similar efficiency to anti-ICAM NCs (Fig. 3). Uptake of anti-ICAM/αGal NCs occurred via CAM endocytosis bypassing clathrin-mediated uptake, which is associated to lysosomal enzymes and may be defective in some cells affected by LSDs [13,54].

We have also shown for the first time that ICAM-1 targeting and CAM-mediated endocytosis in microvascular ECs was similarly efficient to macrovascular ECs described previously [27,34]. Since the microvasculature contains the majority of the endothelial surface in the body, this is a crucial result not only in the context of treatment for Fabry disease but also for ICAM-1-targeted delivery of therapeutic and imaging agents for many other vascular interventions.

Also in animal experiments anti-ICAM/α-Gal NCs targeted organs with efficiency comparable to anti-ICAM NCs (Table 2 and our updated results from [38]). For instance the accumulation of these two formulations were 2.1%ID/g vs 2.5%ID/g in heart and 4.6%ID/g vs 4.4%ID/g in kidney. Accumulation in the liver and spleen was reduced for anti-ICAM/α-Gal NCs vs anti-ICAM NCs (12.4%ID/g vs 43.7%ID/g in liver, 25.7%ID/g vs 56.8%ID/g in spleen) while it was increased in the lungs (175.3%ID/g vs 114.7%ID/g). Targeting to vascular ECs was demonstrated by intravascular perfusion of mice, which did not result in release of nanocarriers accumulated in organs (Fig. S1), and was visualized by TEM (Fig. 2). This is the first description of brain targeting by anti-ICAM NCs, and the first visualization of endothelial targeting and endocytosis of these carriers in the kidney and heart (Fig. 2), critical for treatment of the vasculopathy in these organs due to Fabry disease. Compared to non-targeted α-Gal, anti-ICAM/α-Gal NCs markedly enhanced enzyme delivery to all organs tested, e.g., ~40%, 270%, and 410% increase in kidneys, brain, and heart, main target organs in Fabry disease (Table 2). About 60% of the lung fraction of anti-ICAM/α-Gal NCs redistributed by 24 after injection, in part to the liver and spleen (Fig. S1). This is in contrast to previous results showing lung retention of 75% anti-ICAM NCs [28] and may be due to either lower affinity binding of anti-ICAM/α-Gal NCs carrying lower anti-ICAM surface density than anti-ICAM NCs and/or rapid metabolism of nanoparticles bearing a lysosomal enzyme by vascular ECs in the lung. In any case, the fraction of anti-ICAM/α-Gal NCs retained in the lung still represents 150 fold enhancement in the amount of enzyme delivered to this organ compared to non-targeted α-Gal.

The relative distribution of anti-ICAM/α-Gal NCs among different organs (Table 2) correlated well with the size and vascularization of these organs, e.g., liver and lungs received the maximal fraction of the injected dose. It also correlated with ICAM-1 expression, higher in the liver and lungs, followed by heart, kidney, and spleen [23]. This was also observed in our work where enhanced ICAM-1 expression in lungs of ASM knock out mice resulted in increased pulmonary targeting by anti-ICAM/ASM nanocarriers compared to control mice [23]. ICAM-1 expression in mouse brain, measured in this work, was comparable to heart and kidney (45±5% of the lung level, not shown), correlating with lower nanocarrier accumulation in brain vs lung and liver (Table 2). Higher accumulation of anti-ICAM/α-Gal nanocarriers in spleen vs heart (despite the higher level of ICAM-1 expression in this organ) may be due to high blood shear stress in the heart, which may drag nanocarriers before they can firmly bind to the vascular wall. The spleen is part of the reticuloendothelial system whose fenestrated vessels “filter” particles in circulation too large to be filtered by the kidneys. Macrophages in the spleen may also account for phagocytosis of antibody-coated nanocarriers via Fc recognition of targeting antibodies. Although this may be the case for this anti-ICAM nanocarriers prototype, future nanocarrier coating with polyethylene glycol and substitution of whole anti-ICAM with antibody fragments or affinity peptides (under development) will help minimize retention in the reticuloendothelial system. Yet, α-Gal deficiency affects all organs at some extent and broad targeting would still be beneficial. Ultimately, anti-ICAM nanocarriers provided enhanced α-Gal delivery vs the free enzyme in all organs, including those that are most affected by the disease. Since other cell types, apart from vascular ECs, would also benefit from enzyme delivery, perhaps a combination of free and ICAM-1-targeted enzyme would provide an optimal treatment option.

In vivo distribution of anti-ICAM/α-Gal NCs was somewhat similar to that of anti-ICAM NCs bearing another lysosomal enzyme, ASM, yet with reduced accumulation of anti-ICAM/α-Gal NCs vs anti-ICAM/ASM NCs in liver (12.4%ID/g vs 36.4%ID/g) and spleen (25.7%ID/g vs 47.3%ID/g), and enhanced accumulation in the lungs (175.3%ID/g vs 140.8%ID/g) [23]. In both cases anti-ICAM NCs markedly enhanced the delivery of the cargo enzymes in mice, suggesting that ICAM-1-targeting strategy may represent a suitable platform for general lysosomal enzyme delivery. However, as observed here, it is necessary to test each particular formulation to evaluate their targeting performance. In view of these promising results, future studies will be dedicated to evaluate the therapeutic utility and potential effects of α-Gal delivery by ICAM-1-targeted nanocarriers in the animal model for Fabry disease.

In conclusion, ICAM-1-targeting of α-Gal markedly enhances enzyme delivery to organs in the body and vascular ECs, a main target for treatment of Fabry disease, allowing efficient enzyme uptake, lysosomal delivery, and Gb3 degradation. The optimization of such a strategy may provide a means for improving the therapeutic outcome of enzyme treatments for Fabry disease.

Supplementary Material

Refer to Web version on PubMed Central for supplementary material.

Acknowledgments

The authors thank Wen-An Chiou (Nanocenter, University of Maryland, College Park, MD) and Timothy Maugel (Laboratory for Biological Ultrastructure, University of Maryland, College Park, MD) for technical assistance on preparation and analysis of TEM samples, and Rick John and Jeremy Warren (NanoSight Limited of Salisbury, Wilshire, UK) for providing the size measurement of anti-ICAM/α-Gal NCs.

This work has been funded by Nanobiotechnology Program of the Maryland Department of Business and Economic Development, Minta Martin Foundation, AHA 09BGI2450014, and R01 HL098416 (SM).

References

1. Desnick, RJ.; Ioannou, YA.; Eng, CM. XVI Chapter, Lysosomal Disorders. The Metabolic and Molecular Bases of Inherited Disease. 8. Scriver, C.; Beaudet, A.; Sly, W.; Valle, D.; Childs, B.; Kinzler, K.; Vogelstein, B., editors. McGraw-Hill; 2001.
2. Park JL, Whitesall SE, D'Alecy LG, Shu L, Shayman JA. Vascular dysfunction in the alpha-galactosidase A-knockout mouse is an endothelial cell-, plasma membrane-based defect. Clin Exp Pharmacol Physiol. 2008; 35(10):1156–1163. [PubMed: 18565198]
3. Shu L, Shayman JA. Caveolin-associated accumulation of globotriaosylceramide in the vascular endothelium of alpha-galactosidase A null mice. J Biol Chem. 2007; 282(29):20960–20967. [PubMed: 17535804]
4. Lee K, Jin X, Zhang K, Copertino L, Andrews L, Baker-Malcolm J, Geagan L, Qiu H, Seiger K, Barngrover D, McPherson JM, Edmunds T. A biochemical and pharmacological comparison of enzyme replacement therapies for the glycolipid storage disorder Fabry disease. Glycobiology. 2003; 13(4):305–313. [PubMed: 12626384]
5. Kornfeld S, Reitman ML, Varki A, Goldberg D, Gabel CA. Steps in the phosphorylation of the high mannose oligosaccharides of lysosomal enzymes. Ciba Found Symp. 1982; (92):138–156. [PubMed: 6295719]
6. Neufeld EF. The uptake of enzymes into lysosomes: an overview. Birth Defects Orig Artic Ser. 1980; 16(1):77–84. [PubMed: 7448363]
7. Beck M. Agalsidase alfa for the treatment of Fabry disease: new data on clinical efficacy and safety. Expert Opin Biol Ther. 2009; 9(2):255–261. [PubMed: 19236256]

8. Desnick RJ. Enzyme replacement therapy for Fabry disease: lessons from two alpha-galactosidase A orphan products and one FDA approval. Expert Opin Biol Ther. 2004; 4(7):1167–1176. [PubMed: 15268683]

9. Mehta A, Beck M, Kampmann C, Frustaci A, Germain DP, Pastores GM, Sunder-Plassmann G. Enzyme replacement therapy in Fabry disease: comparison of agalsidase alfa and agalsidase beta. Mol Genet Metab. 2008; 95(1–2):114–115. [PubMed: 18701330]

10. Murray GJ, Anver MR, Kennedy MA, Quirk JM, Schiffmann R. Cellular and tissue distribution of intravenously administered agalsidase alfa. Mol Genet Metab. 2007; 90(3):307–312. [PubMed: 17188539]

11. Koskenvuo JW, Hartiala JJ, Nuutila P, Kalliokoski R, Viikari JS, Engblom E, Penttinen M, Knuuti J, Mononen I, Kantola IM. Twenty-four-month alpha-galactosidase A replacement therapy in Fabry disease has only minimal effects on symptoms and cardiovascular parameters. J Inherit Metab Dis. 2008; 31(3):432–441. [PubMed: 18509742]

12. Schiffmann R, Ries M. Fabry's disease--an important risk factor for stroke. Lancet. 2005; 366(9499):1754–1756. [PubMed: 16298202]

13. Cardone M, Porto C, Tarallo A, Vicinanza M, Rossi B, Polishchuk E, Donaudy F, Andria G, De Matteis MA, Parenti G. Abnormal mannose-6-phosphate receptor trafficking impairs recombinant alpha-glucosidase uptake in Pompe disease fibroblasts. Pathogenetics. 2008; 1(1):6. [PubMed: 19046416]

14. Dhami R, Schuchman EH. Mannose 6-phosphate receptor-mediated uptake is defective in acid sphingomyelinase-deficient macrophages: implications for Niemann-Pick disease enzyme replacement therapy. J Biol Chem. 2004; 279(2):1526–1532. [PubMed: 14557264]

15. Linthorst GE, Hollak CE, Donker-Koopman WE, Strijland A, Aerts JM. Enzyme therapy for Fabry disease: neutralizing antibodies toward agalsidase alpha and beta. Kidney Int. 2004; 66(4):1589–1595. [PubMed: 15458455]

16. Ohashi T, Iizuka S, Ida H, Eto Y. Reduced alpha-Gal A enzyme activity in Fabry fibroblast cells and Fabry mice tissues induced by serum from antibody positive patients with Fabry disease. Mol Genet Metab. 2008; 94(3):313–318. [PubMed: 18456533]

17. Marlin SD, Springer TA. Purified intercellular adhesion molecule-1 (ICAM-1) is a ligand for lymphocyte function-associated antigen 1 (LFA-1). Cell. 1987; 51(5):813–819. [PubMed: 3315233]

18. DeGraba T, Azhar S, Dignat-George F, Brown E, Boutiere B, Altarescu G, McCarron R, Schiffmann R. Profile of endothelial and leukocyte activation in Fabry patients. Ann Neurol. 2000; 47(2):229–233. [PubMed: 10665494]

19. Shen JS, Meng XL, Moore DF, Quirk JM, Shayman JA, Schiffmann R, Kaneski CR. Globotriaosylceramide induces oxidative stress and up-regulates cell adhesion molecule expression in Fabry disease endothelial cells. Mol Genet Metab. 2008; 95(3):163–168. [PubMed: 18707907]

20. Bloemen PG, Henricks PA, van Bloois L, van den Tweel MC, Bloem AC, Nijkamp FP, Crommelin DJ, Storm G. Adhesion molecules: a new target for immunoliposome-mediated drug delivery. FEBS Lett. 1995; 357(2):140–144. [PubMed: 7805880]

21. Chittasupho C, Xie SX, Baoum A, Yakovleva T, Siahaan TJ, Berkland CJ. ICAM-1 targeting of doxorubicin-loaded PLGA nanoparticles to lung epithelial cells. Eur J Pharm Sci. 2009; 37(2): 141–150. [PubMed: 19429421]

22. Finikova OS, Lebedev AY, Aprelev A, Troxler T, Gao F, Garnacho C, Muro S, Hochstrasser RM, Vinogradov SA. Oxygen microscopy by two-photon-excited phosphorescence. Chemphyschem. 2008; 9(12):1673–1679. [PubMed: 18663708]

23. Garnacho C, Dhami R, Simone E, Dziubla T, Leferovich J, Schuchman EH, Muzykantov V, Muro S. Delivery of acid sphingomyelinase in normal and niemann-pick disease mice using intercellular adhesion molecule-1-targeted polymer nanocarriers. J Pharmacol Exp Ther. 2008; 325(2):400–408. [PubMed: 18287213]

24. Murciano JC, Muro S, Koniaris L, Christofidou-Solomidou M, Harshaw DW, Albelda SM, Granger DN, Cines DB, Muzykantov VR. ICAM-directed vascular immunotargeting of

antithrombotic agents to the endothelial luminal surface. Blood. 2003; 101(10):3977–3984. [PubMed: 12531816]

25. Muro S, Gajewski C, Koval M, Muzykantov VR. ICAM-1 recycling in endothelial cells: a novel pathway for sustained intracellular delivery and prolonged effects of drugs. Blood. 2005; 105(2): 650–658. [PubMed: 15367437]
26. Muro S, Garnacho C, Champion JA, Leferovich J, Gajewski C, Schuchman EH, Mitragotri S, Muzykantov VR. Control of endothelial targeting and intracellular delivery of therapeutic enzymes by modulating the size and shape of ICAM-1-targeted carriers. Mol Ther. 2008; 16(8):1450–1458. [PubMed: 18560419]
27. Muro S, Schuchman EH, Muzykantov VR. Lysosomal enzyme delivery by ICAM-1-targeted nanocarriers bypassing glycosylation- and clathrin-dependent endocytosis. Mol Ther. 2006; 13(1): 135–141. [PubMed: 16153895]
28. Rossin R, Muro S, Welch MJ, Muzykantov VR, Schuster DP. In vivo imaging of 64Cu-labeled polymer nanoparticles targeted to the lung endothelium. J Nucl Med. 2008; 49(1):103–111. [PubMed: 18077519]
29. Sakhalkar HS, Dalal MK, Salem AK, Ansari R, Fu J, Kiani MF, Kurjiaka DT, Hanes J, Shakesheff KM, Goetz DJ. Leukocyte-inspired biodegradable particles that selectively and avidly adhere to inflamed endothelium in vitro and in vivo. Proc Natl Acad Sci U S A. 2003; 100(26):15895–15900. [PubMed: 14668435]
30. Villanueva FS, Jankowski RJ, Klibanov S, Pina ML, Alber SM, Watkins SC, Brandenburger GH, Wagner WR. Microbubbles targeted to intercellular adhesion molecule-1 bind to activated coronary artery endothelial cells. Circulation. 1998; 98(1):1–5. [PubMed: 9665051]
31. Weiner RE, Sasso DE, Gionfriddo MA, Thrall RS, Syrbu S, Smilowitz HM, Vento J. Early detection of oleic acid-induced lung injury in rats using (111)In-labeled anti-rat intercellular adhesion molecule-1. J Nucl Med. 2001; 42(7):1109–1115. [PubMed: 11438635]
32. Aird WC. Phenotypic heterogeneity of the endothelium: II. Representative vascular beds. Circ Res. 2007; 100(2):174–190. [PubMed: 17272819]
33. Viemann D, Goebeler M, Schmid S, Nordhues U, Klimmek K, Sorg C, Roth J. TNF induces distinct gene expression programs in microvascular and macrovascular human endothelial cells. J Leukoc Biol. 2006; 80(1):174–185. [PubMed: 16617158]
34. Muro S, Wiewrodt R, Thomas A, Koniaris L, Albelda SM, Muzykantov VR, Koval M. A novel endocytic pathway induced by clustering endothelial ICAM-1 or PECAM-1. J Cell Sci. 2003; 116(Pt 8):1599–1609. [PubMed: 12640043]
35. Gehr P, Bachofen M, Weibel ER. The normal human lung: ultrastructure and morphometric estimation of diffusion capacity. Respir Physiol. 1978; 32(2):121–140. [PubMed: 644146]
36. Higenbottam TW, Laude EA. Endothelial dysfunction providing the basis for the treatment of pulmonary hypertension: Giles F. Filley lecture. Chest. 1998; 114(1 Suppl):72S–79S. [PubMed: 9676644]
37. Jaffe EA. Cell biology of endothelial cells. Hum Pathol. 1987; 18(3):234–239. [PubMed: 3546072]
38. Muro S, Dziubla T, Qiu W, Leferovich J, Cui X, Berk E, Muzykantov VR. Endothelial targeting of high-affinity multivalent polymer nanocarriers directed to intercellular adhesion molecule 1. J Pharmacol Exp Ther. 2006; 317(3):1161–1169. [PubMed: 16505161]
39. Legler G, Pohl S. Synthesis of 5-amino-5-deoxy-D-galactopyranose and 1,5-dideoxy-1,5-imino-D-galactitol, and their inhibition of alpha- and beta-D-galactosidases. Carbohydr Res. 1986; 155:119–129. [PubMed: 3024831]
40. Muro S. New biotechnological and nanomedicine strategies for treatment of lysosomal storage disorders. Wiley Interdiscip Rev Nanomed Nanobiotechnol. 2010; 2(2):189–204. [PubMed: 20112244]
41. Mumtaz S, Bachhawat BK. Enhanced intracellular stability and efficacy of PEG modified dextranase in the treatment of a model storage disorder. Biochim Biophys Acta. 1994; 1199(2): 175–182. [PubMed: 7510128]
42. Stefano JE, Hou L, Honey D, Kyazike J, Park A, Zhou Q, Pan CQ, Edmunds T. In vitro and in vivo evaluation of a non-carbohydrate targeting platform for lysosomal proteins. J Control Release. 2009; 135(2):113–118. [PubMed: 19146893]

43. Steger LD, Desnick RJ. Enzyme therapy. VI: Comparative in vivo fates and effects on lysosomal integrity of enzyme entrapped in negatively and positively charged liposomes. Biochim Biophys Acta. 1977; 464(3):530–546. [PubMed: 836826]
44. Ansari NH, He Q, Cook JD, Wen J, Srivastava SK. Delivery of liposome-sequestered hydrophobic proteins to lysosomes of normal and Batten disease cells. J Neurosci Res. 1997; 47(3):341–347. [PubMed: 9039656]
45. Weissmann G, Bloomgarden D, Kaplan R, Cohen C, Hoffstein S, Collins T, Gotlieb A, Nagle D. A general method for the introduction of enzymes, by means of immunoglobulin-coated liposomes, into lysosomes of deficient cells. Proc Natl Acad Sci U S A. 1975; 72(1):88–92. [PubMed: 1054517]
46. El-Sayed ME, Hoffman AS, Stayton PS. Smart polymeric carriers for enhanced intracellular delivery of therapeutic macromolecules. Expert Opin Biol Ther. 2005; 5(1):23–32. [PubMed: 15709907]
47. Langer R. Drug delivery and targeting. Nature. 1998; 392(6679 Suppl):5–10. [PubMed: 9579855]
48. Panyam J, Labhasetwar V. Biodegradable nanoparticles for drug and gene delivery to cells and tissue. Adv Drug Deliv Rev. 2003; 55(3):329–347. [PubMed: 12628320]
49. Torchilin VP. Multifunctional nanocarriers. Adv Drug Deliv Rev. 2006; 58(14):1532–1555. [PubMed: 17092599]
50. De Vocht C, Ranquin A, Willaert R, Van Ginderachter JA, Vanhaecke T, Rogiers V, Versees W, Van Gelder P, Steyaert J. Assessment of stability, toxicity and immunogenicity of new polymeric nanoreactors for use in enzyme replacement therapy of MNGIE. J Control Release. 2009; 137(3): 246–254. [PubMed: 19371766]
51. Sahay G, Alakhova DY, Kabanov AV. Endocytosis of nanomedicines. J Control Release. 2010; 145(3):182–195. [PubMed: 20226220]
52. Torchilin VP. Intracellular delivery of protein and peptide therapeutics. Drug Discovery Today: Technologies. 2008; 5(2–3):e95–e103.
53. Mundargi RC, Babu VR, Rangaswamy V, Patel P, Aminabhavi TM. Nano/micro technologies for delivering macromolecular therapeutics using poly(D,L-lactide-co-glycolide) and its derivatives. J Control Release. 2008; 125(3):193–209. [PubMed: 18083265]
54. Dhami R, Passini MA, Schuchman EH. Identification of novel biomarkers for Niemann-Pick disease using gene expression analysis of acid sphingomyelinase knockout mice. Mol Ther. 2006; 13(3):556–564. [PubMed: 16214420]

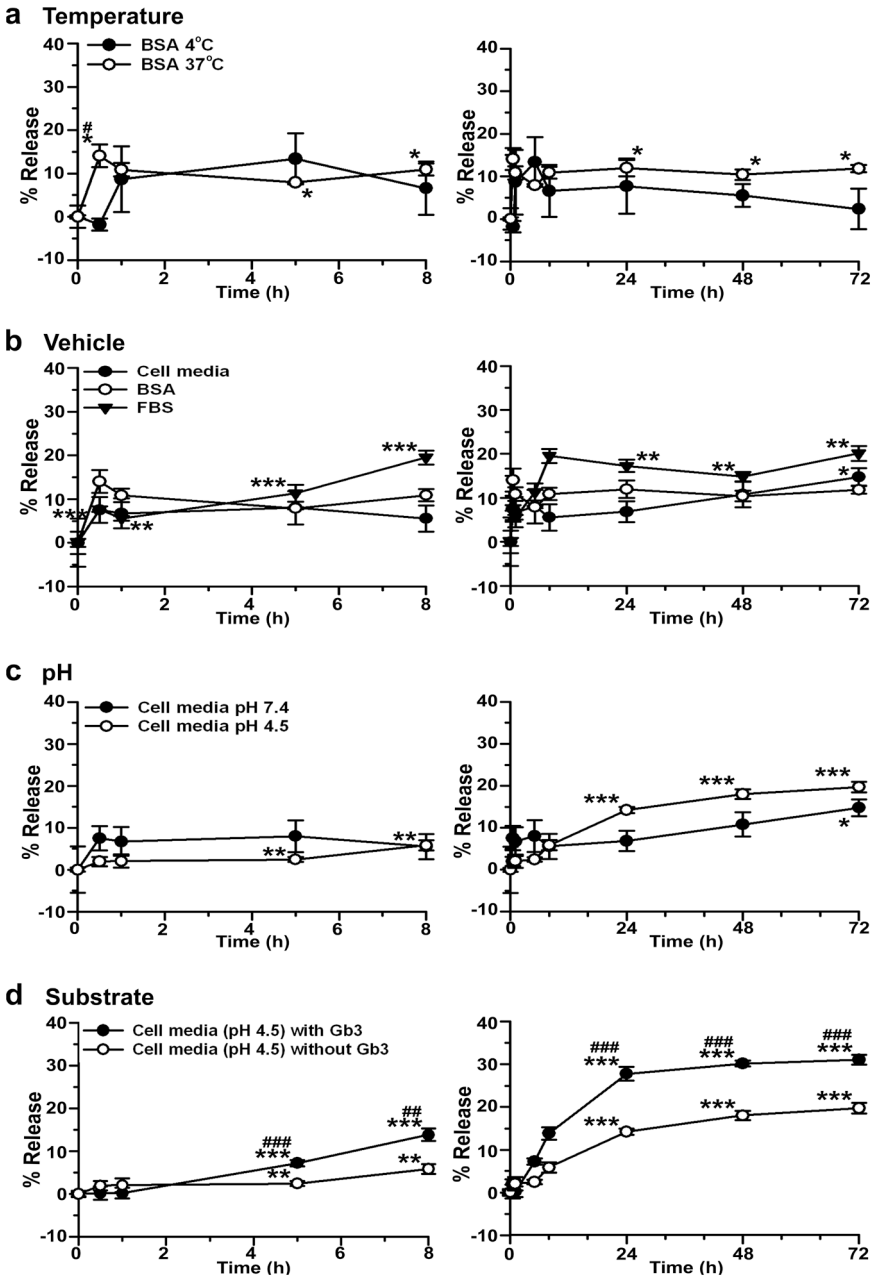

Figure 1. Release of α-Gal from anti-ICAM nanocarriers

^{125}I-α-Gal released from anti-ICAM/^{125}I-α-Gal NCs was separated from the particle-bound fraction by centrifugation after incubation for varying periods of time in **(a)** 1% BSA in PBS buffer at 4°C or 37°C; **(b)** 1% BSA in PBS, HUVEC medium, or FBS at 37°C and pH 7.4; **(c)** HUVEC medium at 37°C and either pH 7.4 or pH 4.5; and **(d)** HUVEC medium at 37°C and pH 4.5 in the absence or presence of NBD-Gb3. Data are mean±SEM (n≥3). * compares each time point to time 0 within the same condition. # compares (for each time point): **(a)** 4°C to 37°C, **(b)** HUVEC medium and FBS to BSA, **(c)** pH 4.5 to pH 7.4, and **(d)** Gb3 to non-Gb3. * and # are $p \leq 0.05$; ** and ## are $p \leq 0.01$; *** and ### are $p \leq 0.001$, by Student's *t*-test. Statistical significance for time 0–8 h are shown only in the left panel and time 24–72 h only in the right panel.

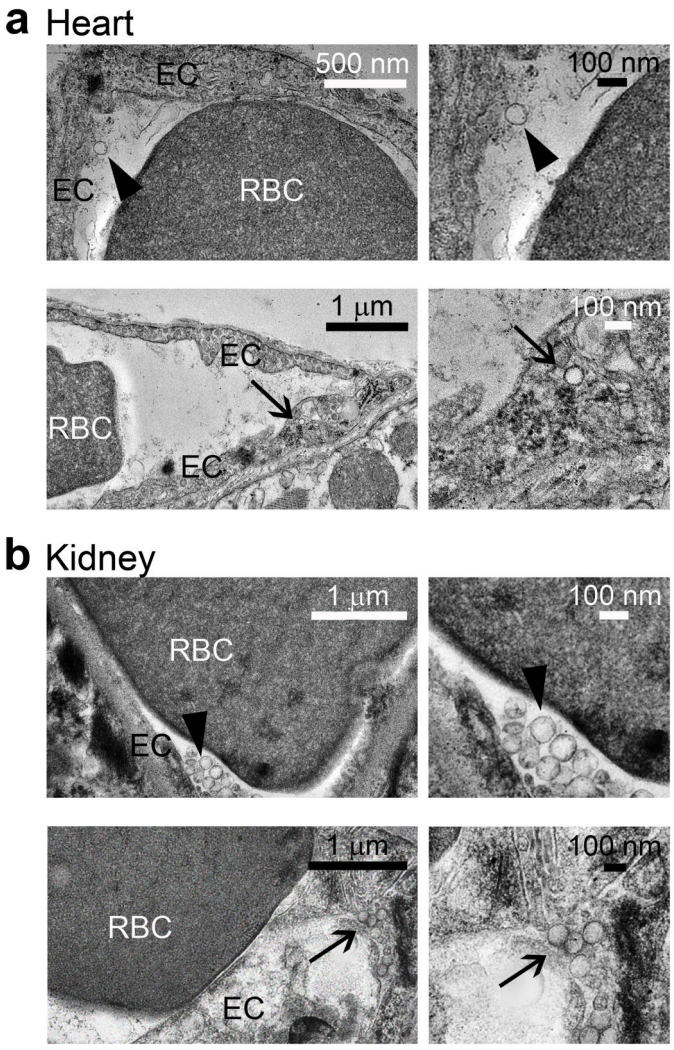

Figure 2. Visualization of anti-ICAM/α-Gal nanocarriers in mice

Transmission electron micrographs showing the presence of anti-ICAM/α-Gal NCs in **(a)** heart and **(b)** kidney, both attached to the endothelial surface (arrowheads, upper panels) and internalized within cells (arrows, bottom panels) by 30 min after injection.

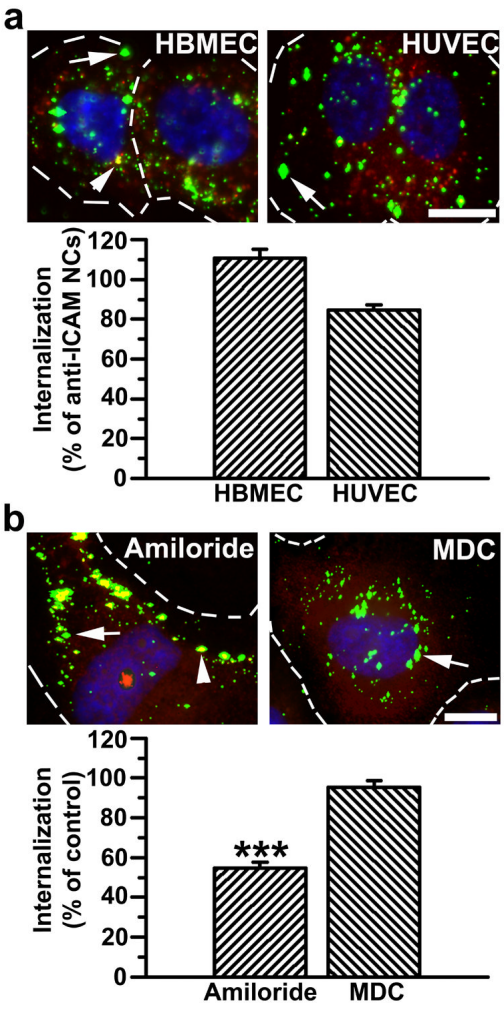

Figure 3.

Efficient targeting and internalization of anti-ICAM/α-Gal nanocarriers in micro- and macro-vascular endothelial cells. (a) Fluorescence microscopy images and quantification of TNFα-activated HBMECs and HUVECs incubated with FITC-labeled anti-ICAM/α-Gal NCs at 37°C for 30 min, washed and incubated in cell medium for 30 min. Cells were fixed and surface-bound NCs and nuclei were stained with Texas-Red-labeled anti-mouse IgG and DAPI, respectively. Internalization was compared to that of anti-ICAM NCs, shown in Figure S2. (b) Uptake of anti-ICAM/α-Gal NCs was also tested in the presence of amiloride or MDC, which inhibit CAM- vs clathrin-mediated endocytosis, respectively. In both (a) and (b), single-labeled green NCs are internalized (arrow) vs double-labeled (green+red) yellow NCs, which are located in the cell surface (arrowhead). Dashed lines mark the cell border, determined by phase-contrast. Scale bar, 10 μm. Data are mean±SEM (n≥55 cells, duplicated). *** is $p \leq 0.001$, by Student's *t*-test.

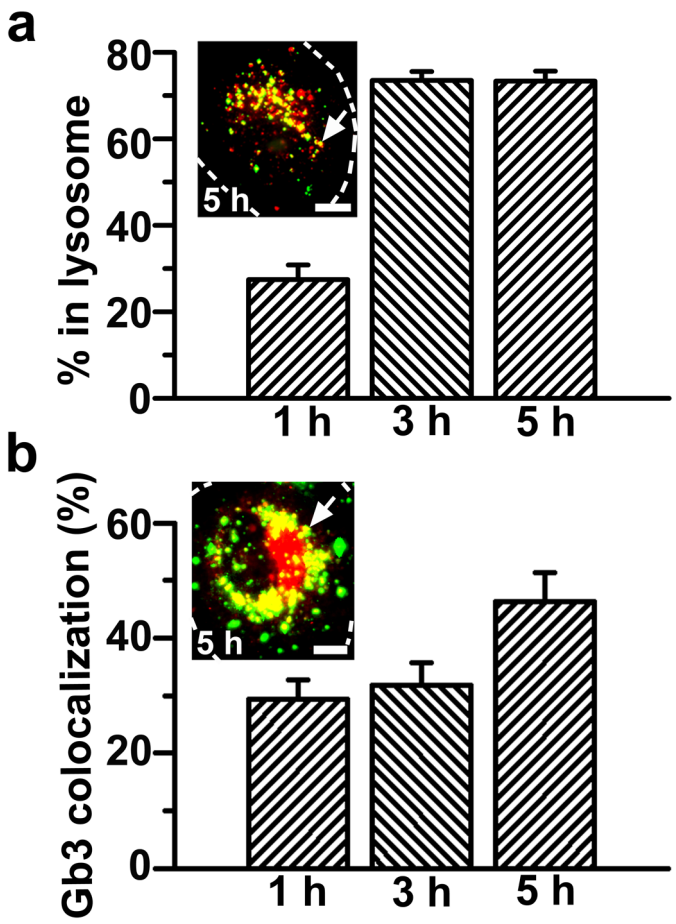

Figure 4. Internalized anti-ICAM/α-Gal nanocarriers traffic to lysosomes and colocalize with Gb3

(a) TNFα-activated HUVECs were incubated at 37°C for 1 h with Texas-Red dextran to label lysosomes, followed by incubation with FITC-labeled anti-ICAM/α-Gal NCs for 1 hour at 37°C. Cells were washed and fixed, or washed and incubated with cell medium for 2 or 4 additional hours (total incubation time: 1, 3, and 5 h) and then fixed. **(b)** Cells were incubated for 16 h with DGJ and NBD-Gb3 to visualize accumulation of this green-fluorescent substrate analog in intracellular compartments (red pseudocolor) and then incubated with non-fluorescent anti-ICAM/α-Gal NCs as in **a**. Cells were then washed, fixed, and permeabilized, and NCs were stained with Texas-Red-labeled goat anti-mouse IgG (green pseudocolor). Samples were analyzed by fluorescence microscopy to determine the percentage of (pseudo) green-labeled NCs which colocalized within (pseudo) red-labeled lysosomes or Gb3-positive compartments (yellow, arrows). Dashed lines mark the cell borders, determined by phase-contrast. Scale bar, 10 μm. Data are mean±SEM (n≥23 cells, duplicated).

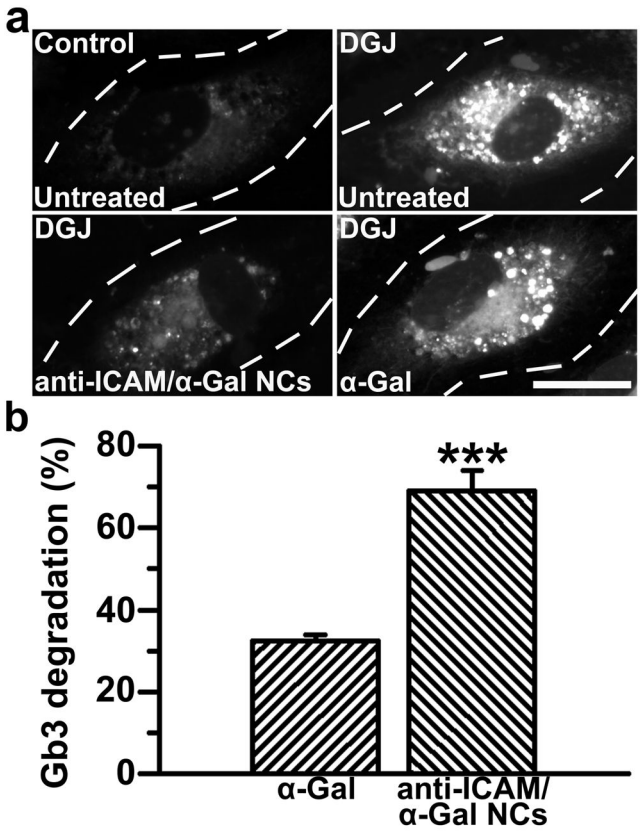

Figure 5. Anti-ICAM/α-Gal nanocarriers attenuate Gb3 accumulation in an endothelial cell model of Fabry disease

(a) TNFα-activated HUVECs were incubated at 37°C for 16 h with fluorescent NBD-Gb3 and control cell medium or medium containing DGJ to inhibit endogenous αGal. Cells were then washed and left untreated or treated with α-Gal or non-fluorescent anti-ICAM/α-Gal NCs for 5 h, all in the presence of chloroquine to selectively permit activity of exogenous neutral α-Gal, and not endogenous acidic α-Gal. Cells were fixed and analyzed by fluorescence microscopy. Dashed lines mark cell borders, determined by phase-contrast. Scale bar, 10 μm. **(b)** Intracellular accumulation of NBD-Gb3 was quantified from micrographs as described in Materials and Methods. Data are mean±SEM (n≥72 cells). *** is $p \leq 0.001$, by Student's *t*-test.

Table 1

Circulation of anti-ICAM/α-Gal nanocarriers vs α-Gal in mice

	%ID in blood		
	1 minute	15 minutes	30 minutes
Anti-ICAM/α-Gal NCs	5.85±0.67[a]	3.86±0.40[a]	5.59±0.33[a]
α-Gal	64.72±3.96	44.40±3.34	42.07±2.22

%ID = percentage of injected dose

Data are mean±SEM, n≥8 mice.

[a] is $p<0.001$, by Student's *t*-test.

Table 2

Biodistribution of anti-ICAM/α-Gal nanocarriers vs α-Gal in mice

	Brain		Heart		Kidney		Liver		Lung		Spleen	
	α-Gal NCs	**α-Gal**	**α-Gal NCs**	**α-Gal**	**α-Gal NCs**	**α-Gal**	**α-Gal NCs**	**α-Gal**	**α-Gal NCs**	**α-Gal**	**α-Gal NCs**	**α-Gal**
%ID	0.13±0.01	0.25±0.01	0.33±0.04^a	0.49±0.06	1.89±0.14^b	10.12±0.77	18.41±1.22^b	6.68±0.56	36.24±3.47^b	0.74±0.07	3.11±0.43^b	0.40±0.03
%ID/g	0.28±0.02^b	0.56±0.03	2.12±0.32^a	3.23±0.30	4.58±0.32^b	24.58±1.49	12.36±0.71^b	4.48±0.40	175.34±21.41^b	3.80±0.33	25.69±2.78^b	3.66±0.27
LR	0.11±0.02^b	0.03±0.002	0.82±0.17^b	0.16±0.01	1.71±0.12	1.21±0.06	4.76±0.51^b	0.22±0.01	70.07±12.02^b	0.19±0.02	9.32±1.48^b	0.18±0.01
SI	3.67		5.13		1.41		21.64		368.79		51.78	

%ID = percentage of injected dose, %ID/g = % ID per gram of tissue, LR = localization ratio, ratio of %ID/g of tissue to %ID/g of blood, SI = specificity index, calculated as the ratio of LR in an organ for the NC formulation vs the non-targeted enzyme. Organs were collected 30 min after injection. Data are mean±SEM, n≥8 mice.

^{a}is $p<0.05$,

^{b}is $p<0.001$, by Student's *t*-test.